VDE-Related Topics

C. R. Sovinec, K. J. Bunkers,
and B. S. Cornille

University of Wisconsin-Madison

Meeting of the Center for Extended MHD

November 15, 2015

Savannah, Georgia

Outline

- Boundary conditions
  - Follow-up on parallel flow effects
  - New project
- Free-boundary equilibria
- External kink computations
- Summary

- NIMROD-related APS-DPP presentations

Boundary conditions: We have compared conditions on *n* and **V** in a horizontally unstable configuration.

- Initial conditions are from a fixed-boundary G-S computation.
- External region has a horseshoe shape.
- Decay of initial eddy currents allows axisymmetric displacement.
- Along the resistive wall, computations use one of:

  1) $\mathbf{V} = 0$

  2) $\hat{\mathbf{n}} \cdot \mathbf{V} = \hat{\mathbf{n}} \cdot \dfrac{1}{B^2} \mathbf{E}_w \times \mathbf{B}$

  3) $\hat{\mathbf{n}} \cdot \nabla V_n \rightarrow 0 \quad \text{via}$

$$\frac{dV_n}{dt} = -\nu_{Vn} \left(\hat{\mathbf{n}} \cdot \nabla V_n \right) \left[\frac{\delta \left(\hat{\mathbf{n}} \cdot \nabla V_n \right)}{\delta V_n} \right]^{-1}$$

- Conditions on *n* are Dirichlet or as governed by advective flux.

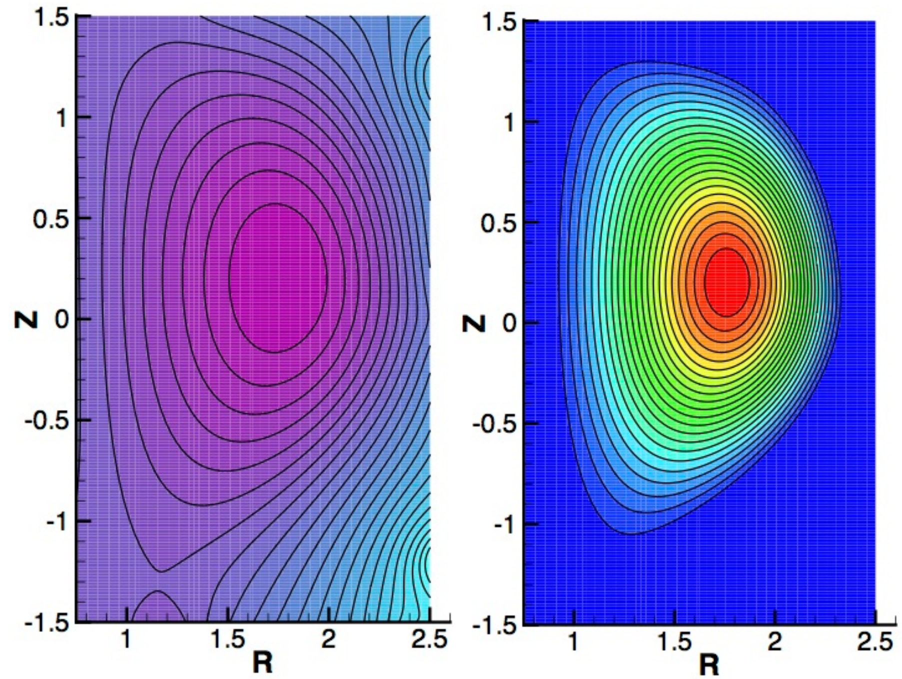

Poloidal flux (left) and pressure (right) for the initial conditions.

- τ_r for the initial profile is of order 10^5.
- With $\eta_w/\mu_0 \delta x = 10^{-3}$, $\tau_w \sim 10^3$.

Displacement from the decay of eddy currents is primarily radial in these cases.

- This configuration has an attracting coil at R=2.6, Z=0 (triangularity) between vertical-field coils at Z=±1.2.
- Edge plasma cools through contact with the wall as the configuration changes from diverted to limited.

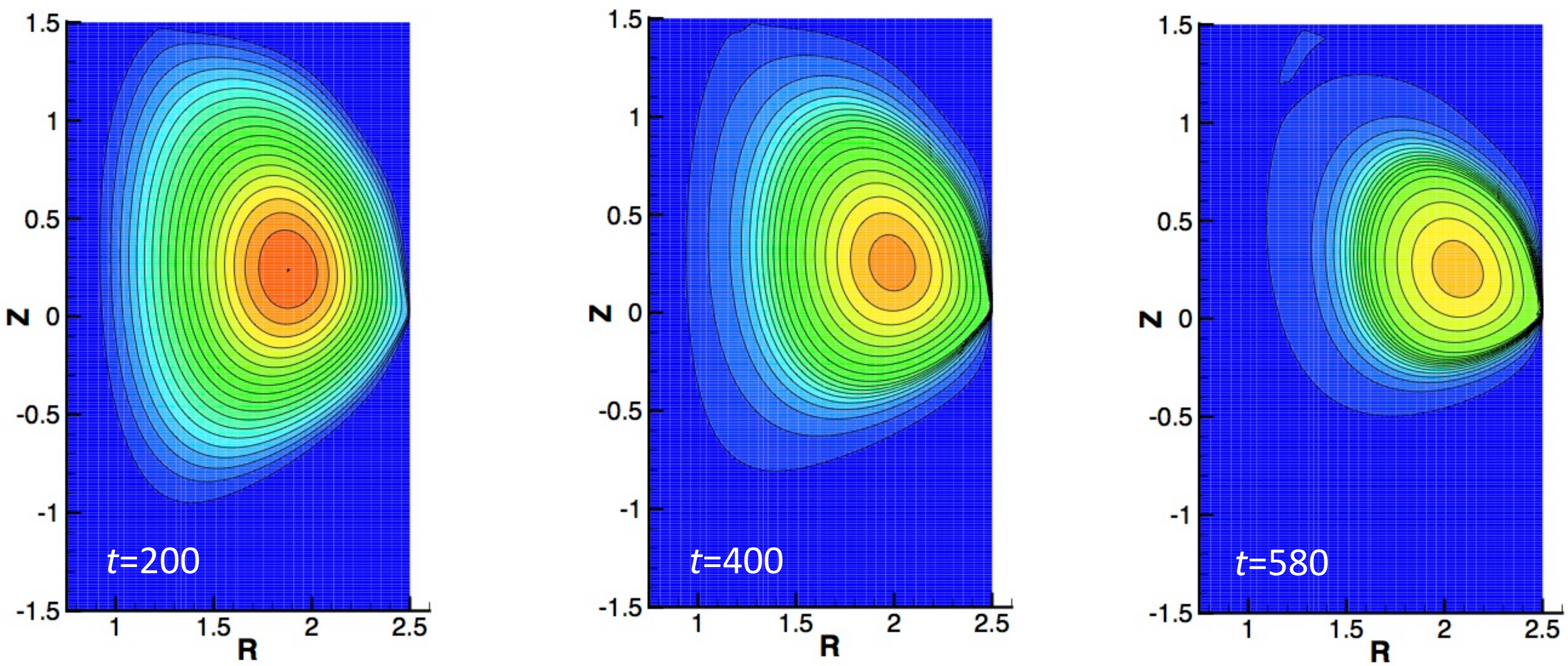

Contours of temperature (same scale for all times) show that confinement remains intact for a central core region.

Parallel flow along open surfaces is accelerated by thermal pressure.

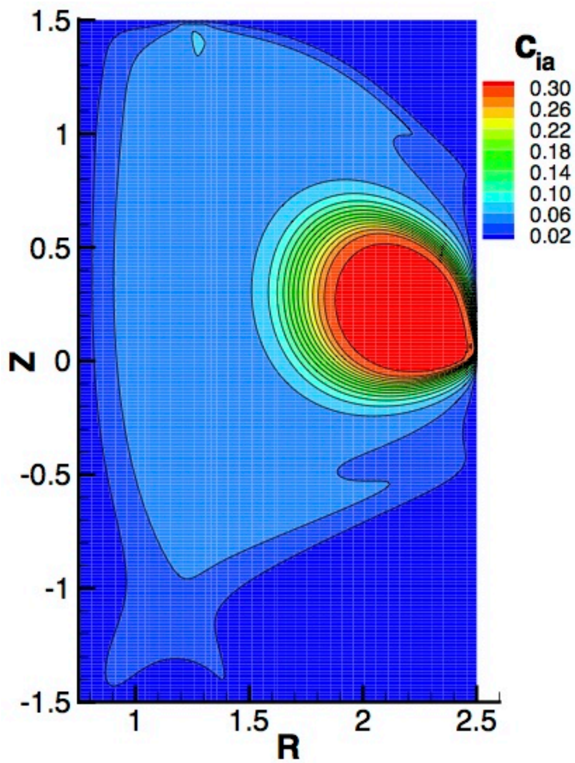

Contours ion-acoustic speed at 900 τ_A show a confined region and a remnant.

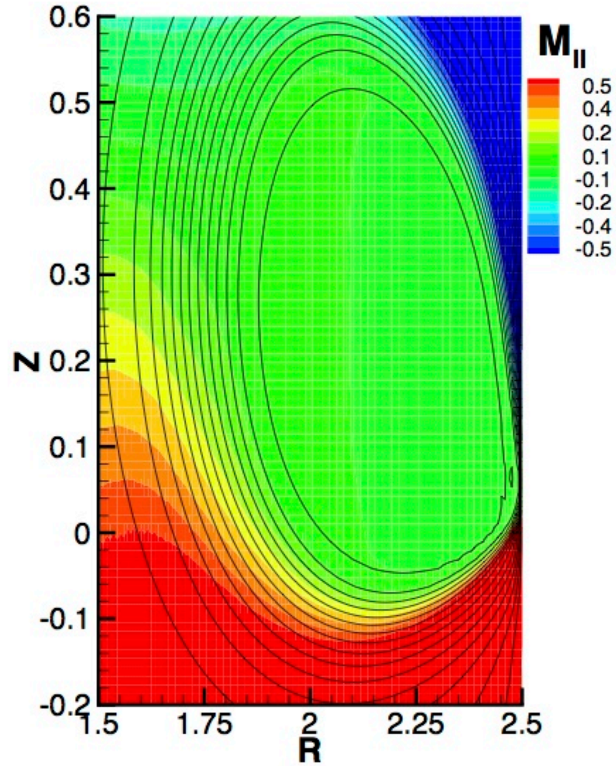

Near-sonic parallel flow develops around confined region; color=$M_{||}$, lines=c_{ia}.

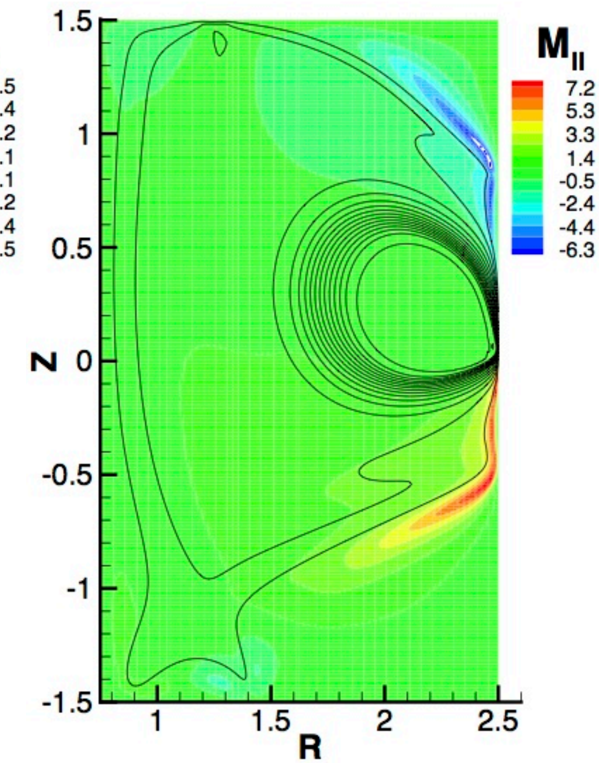

Low-density flow from the remnant becomes supersonic when cooled.

- Plasma inertia is important for the open-field parallel flow.
- A parameter scan finds that flows in the remnant region are sensitive to thermal conductivity and viscosity.

Accumulation of mass along the surface is large with either of the advective mass flux conditions.

- The computation with V_n = 0 has Dirichlet conditions on n, and mass is lost via $\hat{\mathbf{n}} \cdot \Gamma_D = -\hat{\mathbf{n}} \cdot \left(D_n \nabla n - D_h \nabla \nabla^2 n \right)$.
- Mass flow through the boundary is set by $\hat{\mathbf{n}} \cdot \Gamma = \hat{\mathbf{n}} \cdot \left(n\mathbf{V} \right)$ in the computations with the drift-flow and $\hat{\mathbf{n}} \cdot \nabla V_n \rightarrow 0$ conditions.

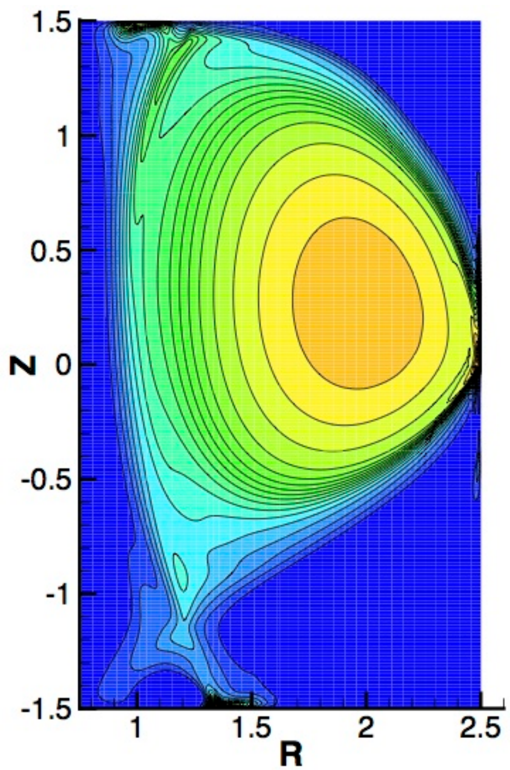

Density at 300 τ_A with V_n=0 and diffusive particle flux.

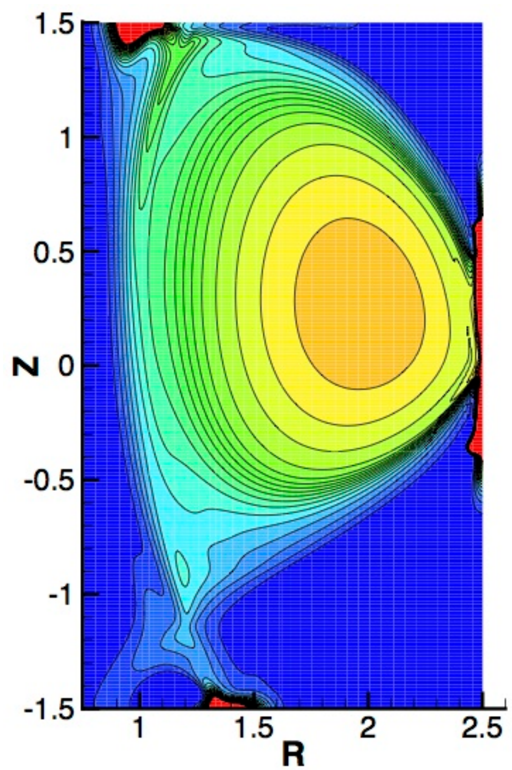

Density at 300 τ_A with E_w×B outflow and advective flux.

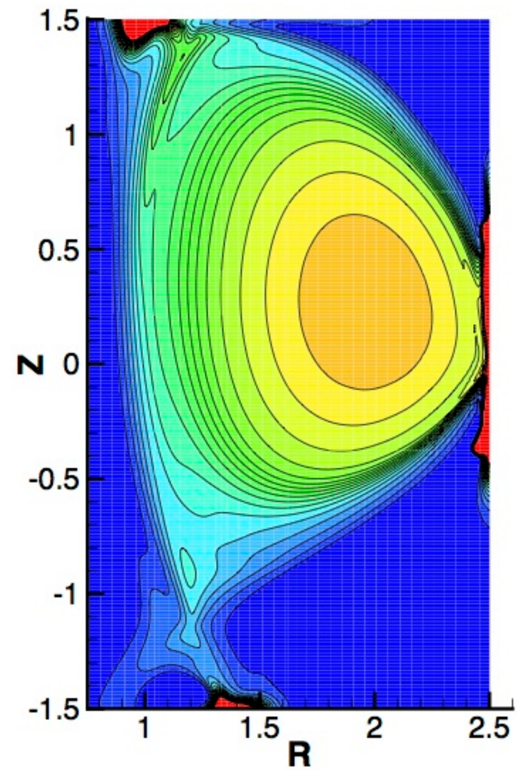

Density at 300 τ_A with n.grad(V_n)->0 and adv. flux.

However, evolution of current and thermal energy is essentially the same when changing among the three conditions on V_n along the wall.

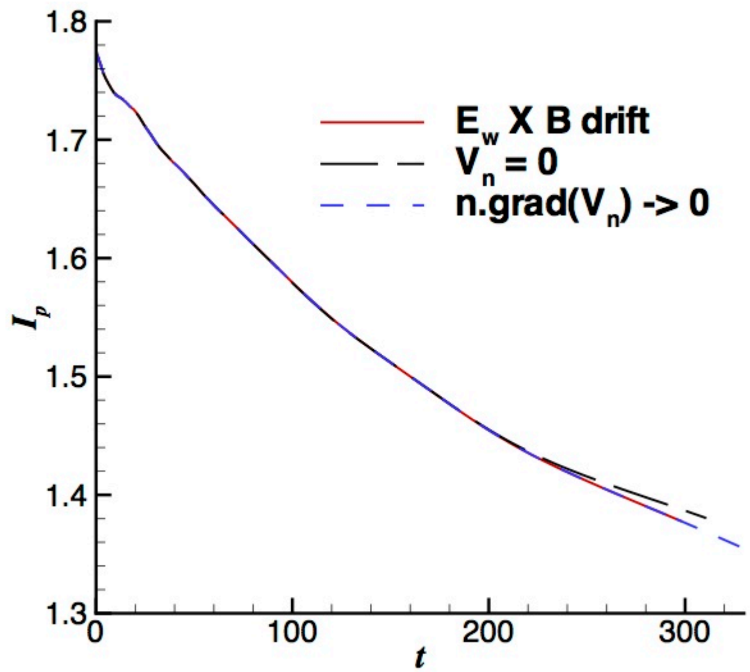

Plasma current traces nearly overlie through 300 τ_A.

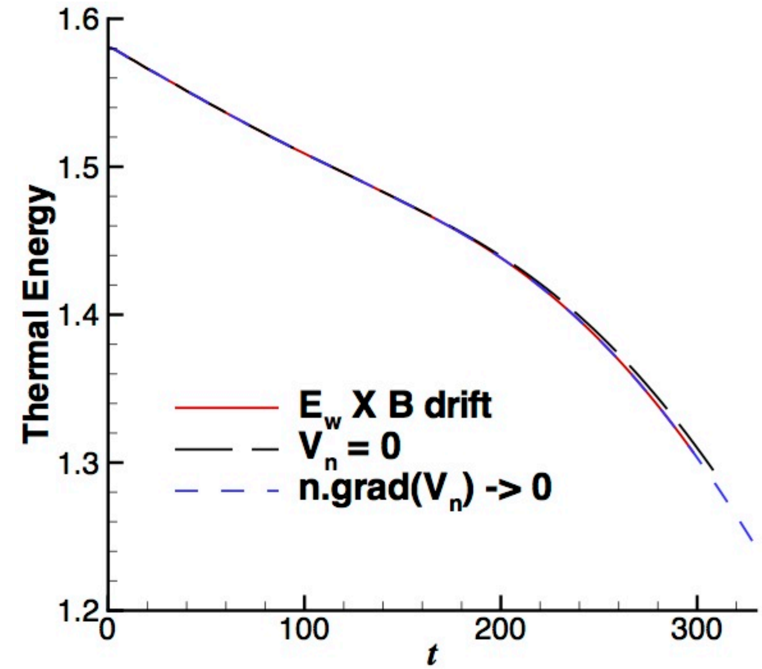

The internal energy traces all show faster decay after the initial phase.

- Flow is primarily along open **B**-field lines after contact with the wall.
- The sonic parallel flow and mass have little effect on flux diffusion through the resistive wall.
- A pre-sheath-like condition worth comparing is uniform $nV_{||}$ along **B.**

A new project is considering how to implement realistic sheath conditions for disruption dynamics.

- Brian Cornille is reviewing literature on magnetized sheath boundary conditions that are used in edge-plasma simulations.
  - Many previous developments (Stangeby and Chankin, PoP 2; Cohen and Ryutov, PoP 6; etc.) consider axisymmetric conditions.
  - More recent studies develop 3D boundary conditions for edge turbulence computation (for example, Loizu, et al., PoP19).
- One dimensional computations provide test and boundary conditions.

- The example result for V_x on the right is for viscous conditions with large pressure on the left side.
  - Unintended pressure from magnetic field that is perpendicular to the flow affects the nimrod plot.

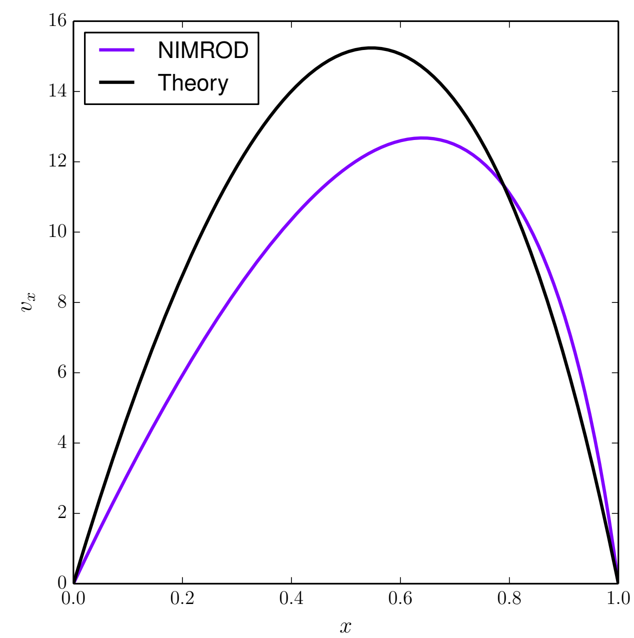

Free-boundary equilibria: Outer-loop updates of surface flux leads to slow convergence for NIMEQ.

- The outer-loop approach[1] treats boundary-flux as fixed at each iterate of an outer loop, then updates based on the latest solution.
- The initial NIMEQ free-boundary implementation uses this method.
- Boundary updates reintroduce large residuals for NIMEQ.
- With outer-loop updates, this double-null equilibrium only achieves a relative tolerance of 10^{-3} after 253 total nonlinear iterations.
- The largest residual values are along the wall.

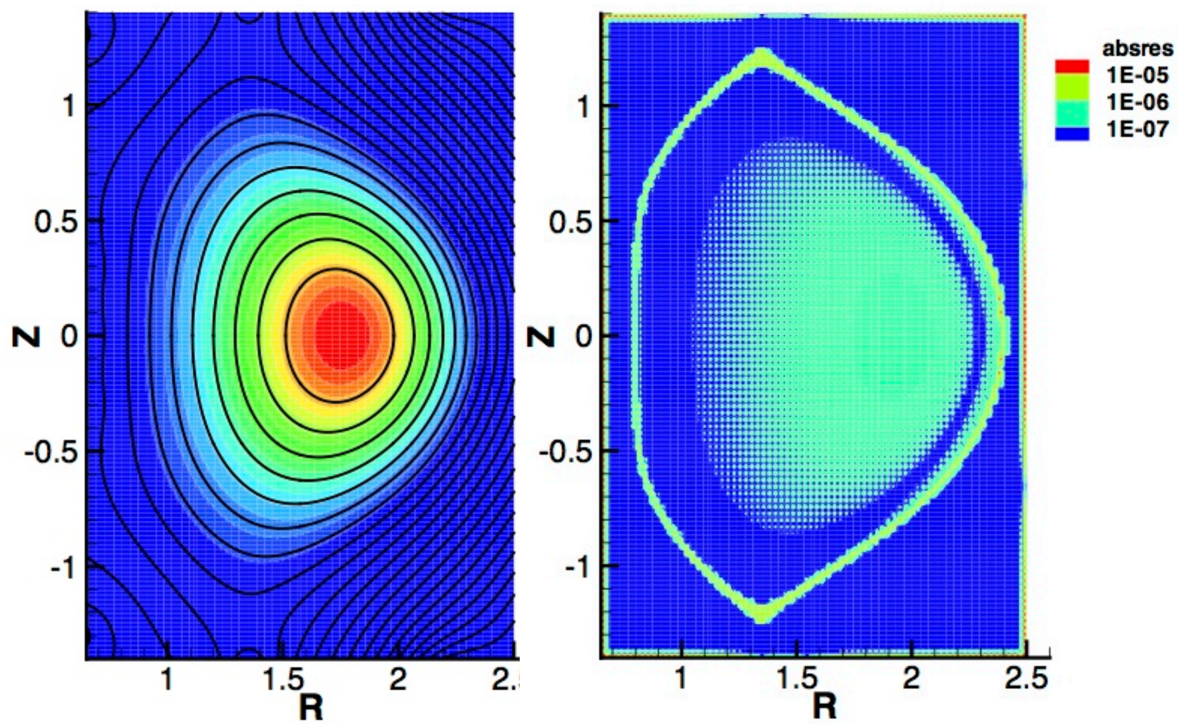

Pressure and poloidal flux. **Residual on exp. scale.**

[1]For example, S. Jardin, *Computational Methods in Plasma Physics*, CRC 2010.

Finding nodal expansions of $\mu_0 j_\phi/R$ and NIMEQ's Λ simultaneously allows us to put surface flux in the linear algebraic system for each nonlinear iteration.

- Analytically, the 2-vector PDE system is redundant:

$$\nabla\cdot R^2\nabla\Lambda = -FF' - \mu_0 R^2 P' \qquad\qquad \Lambda \equiv \Psi/R^2$$
$$R^2\left(\mu_0 j_\phi/R\right) = -FF' - \mu_0 R^2 P'$$

- With C^0 expansions over our elements, solving coefficients for $\mu_0 j_\phi/R$ is necessary to evaluate surface-Λ values for an existing $FF' + \mu_0 R^2 P'$.
- This arises when solving the linear $\nabla\cdot R^2\nabla$ operation at each nonlinear iteration step.
- The left side of the $\mu_0 j_\phi/R$ equation is a projection operation (mass matrix).
- The surface-Λ coefficients are now part of the algebraic system. Including current from the external coils (I_c) and internal current density coefficients, each surface node m requires

$$\Lambda_m - \sum_n \left(\underline{\underline{\hat{M}}}\right)_{mn}\left(\mu_0 j_\phi/R\right)_n = \sum_c \left(\underline{\underline{\breve{M}}}\right)_{mc}\left(\mu_0 I\right)_c$$

The algebraic system is asymmetric, and the rows for surface-Λ coefficients are dense.

- The system is asymmetric, because the surface-Λ coefficients do not have corresponding matrix elements in the $\mu_0 j_\phi / R$ rows.
- A new program module solves the 2D real asymmetric systems.
- Standard NIMROD data structures do not handle dense matrices, so the matrix-vector products are computed as 'matrix-free' operations.
  - The $\mu_0 j_\phi / R$ values are interpolated to the Gaussian quadrature points as part of the surface-Λ row operations.
  - Preconditioning uses our standard methods (SuperLU, diagonal, etc.) for the sparse part of the matrix.

This modification improves free-boundary NIMEQ convergence significantly.

- For the double-null computation, the solve achieves a tolerance of 10^{-3} in 95 nonlinear iteration steps and 10^{-6} in 191.
- The number of GMRES iterations per nonlinear iteration step decreases significantly after the initial nonlinear steps.
- Residual values near the surface do not dominate convergence.

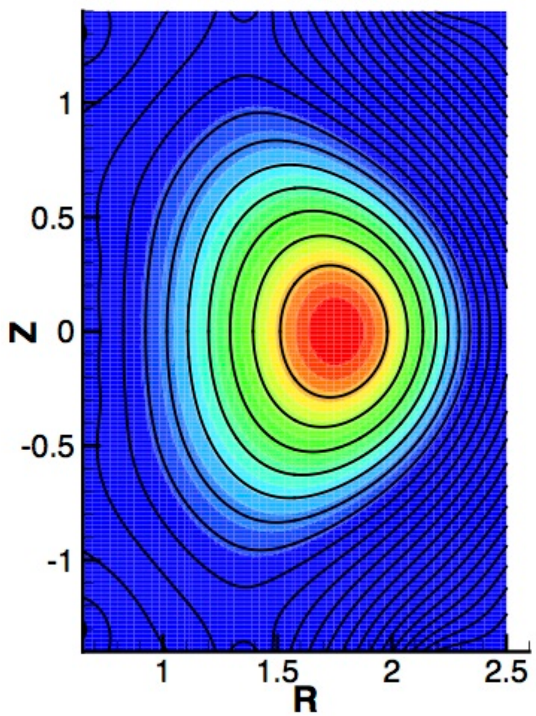

Pressure and poloidal flux.

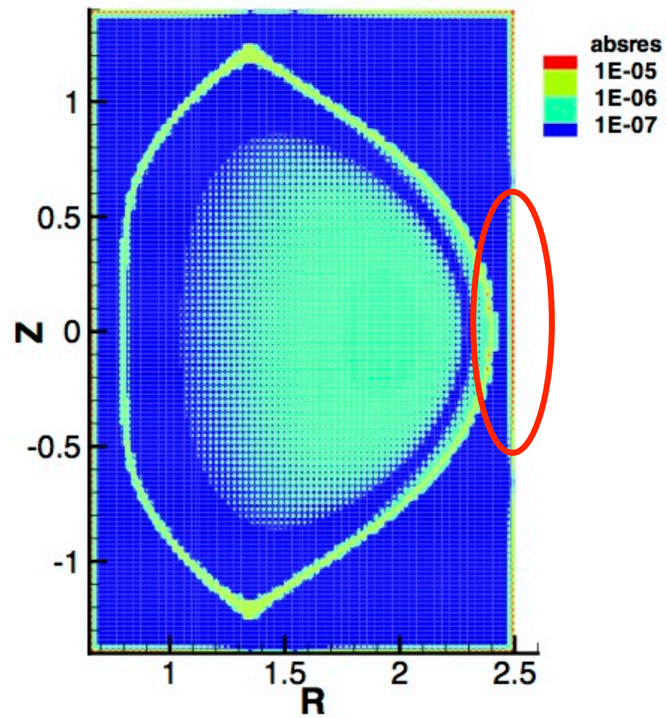

Residual from step 253 of outer-loop method.

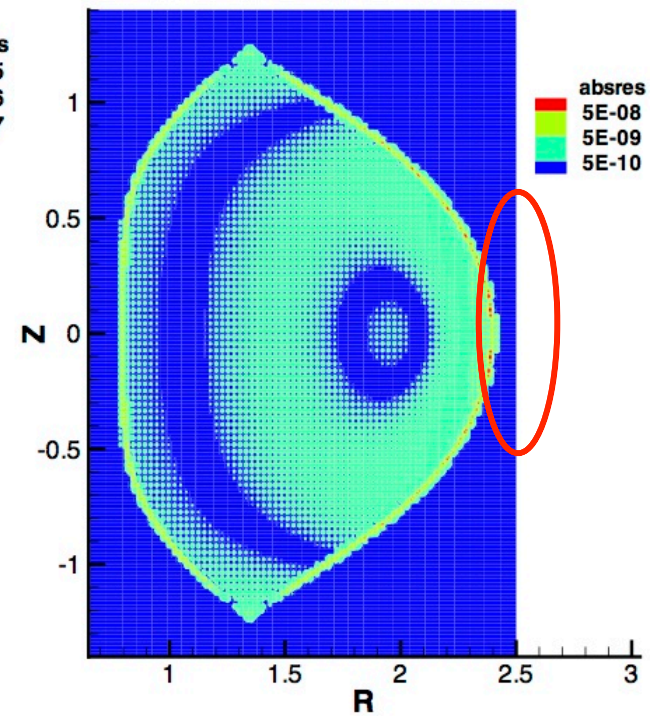

Residual from step 191 of new 2-vector method.

External-kink computations: Our initial focus is numerical resolution when using $\eta(T)$ to distinguish plasma.

- Cylindrical cases consider the classic uniform-J_z equilibrium at large aspect ratio (10).
- We had previously benchmarked linear NIMROD computations when testing the resistive wall implementation (Sherwood, 2014 poster).
- Nonlinear computations need to maintain an accurate representation of the plasma-surface interface through large-amplitude distortion.
    - Cases such as the one on the right have q_{pl} = 1.8.

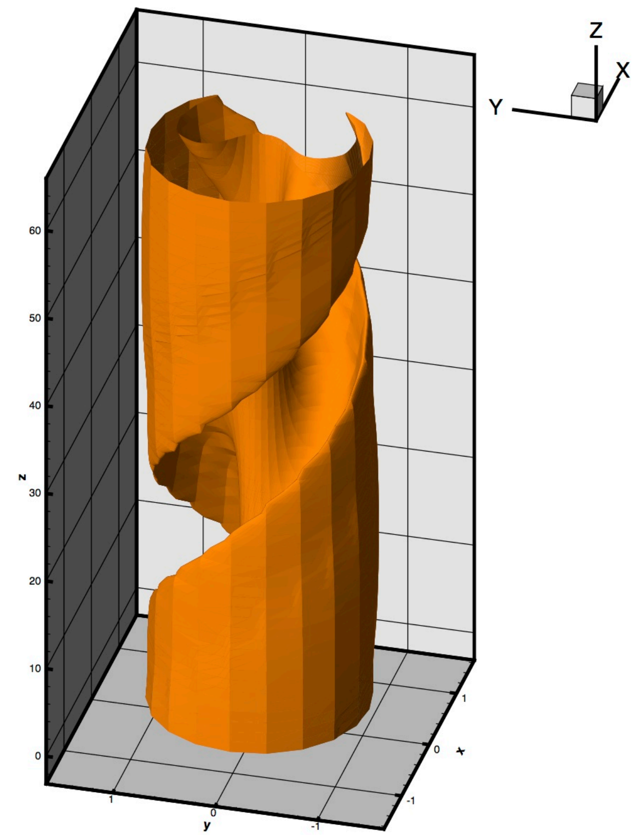

Keeping even-*m* azimuthal components, we find that 0≤*m*≤42 is needed for large-amplitude evolution (Bunkers, NP12.00014).

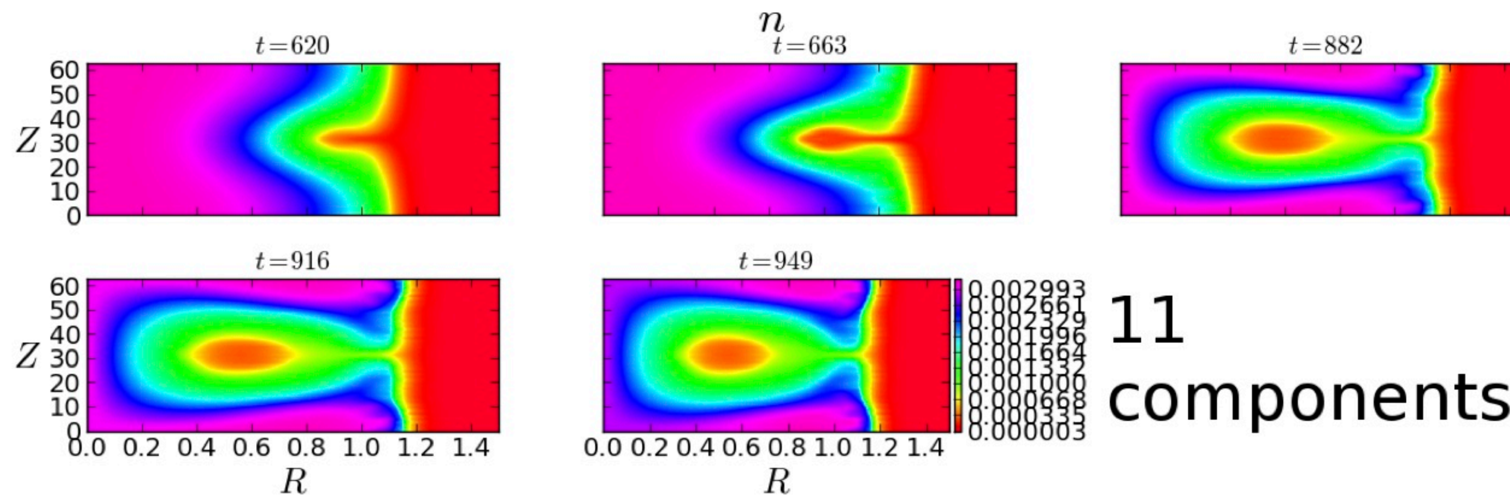

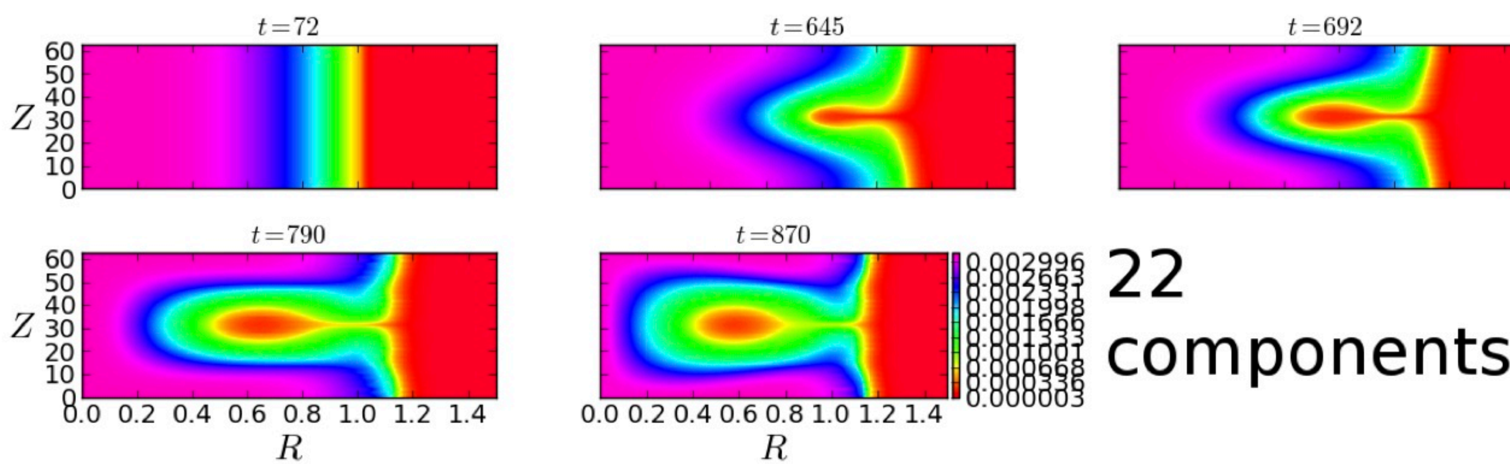

- We can see the instability, which looks like a vacuum bubble[1].

[1] Rosenbluth, Monticello, Strauss and White, Phys. Fluids **19** (1976)

We have also demonstrated nonlinear external kink in toroidal geometry.

- The computations start from a limited free-boundary equilibrium.
- Unlike the cylindrical computations, NIMROD;s Fourier representation is used for the toroidal direction (here, $0 \le n \le 22$).
- The most challenging aspect of the computations is solving the 3D algebraic system for **B** with η varying over 6 orders of magnitude.

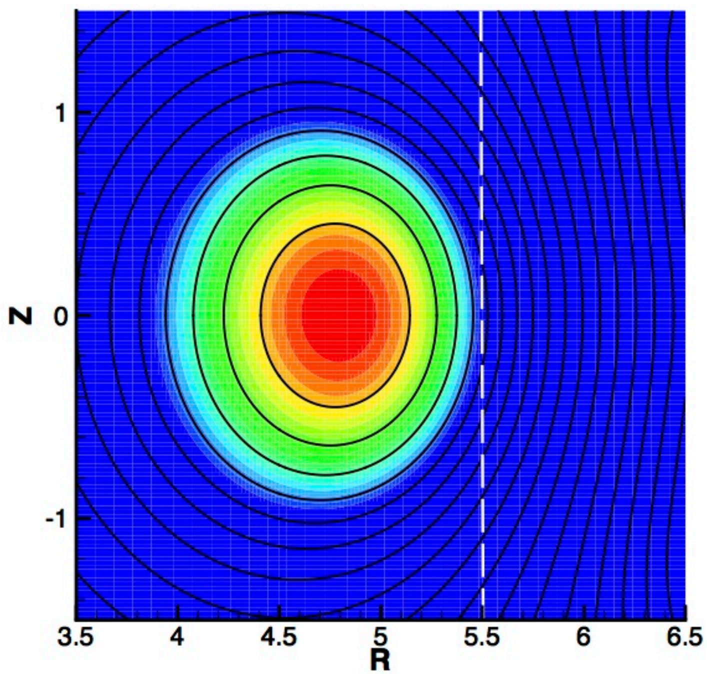

Pressure and poloidal flux. White dashed line shows limiting radius.

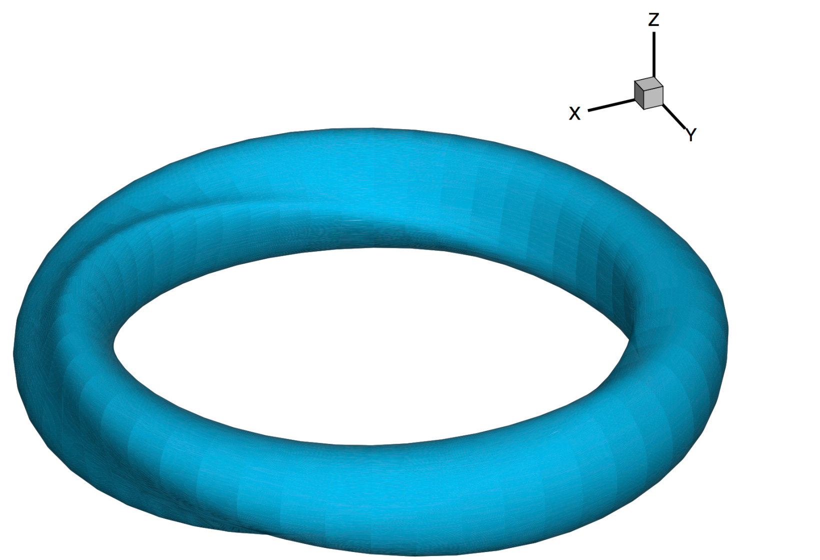

Nonlinear evolution from this equilibrium demonstrates toroidal external kink.

Summary

- We are working on multiple aspects of VDE simulation to study three-dimensional evolution in more representative configurations.
    - Boundary conditions
    - Initialization from free-boundary equilibria
    - Nonlinear external kink
- Assembling these pieces for full VDE/external kink evolution is the next major step.
- Algebraic solvers are (again) the most significant numerical concern.

- NIMROD-related APS presentations (with non-trivial NIMROD contributions) are on the next slide.

NIMROD-Related Presentations at APS-DPP, 2015

1. R Milroy, BP12.00010 : NIMROD simulations of the IPA FRC experiment
2. S Woodruff, BP12.00039 : Design Point for a Spheromak Compression Experiment
3. JB O'Bryan, BP12.00040 : Numerical investigation and optimization of multi-pulse CHI spheromak performance
4. D Lemmon, BP12.00041 : Development of Synthetic Diagnostics for use in Validation
5. JE Stuber, BP12.00042 : 3D MHD Simulations of Spheromak Compression
6. M Christenson, BP12.00043 : On the development of a compact toroid injector at the University of Illinois at Urbana-Champaign
7. K Morgan, BP12.00047 : NIMROD Modeling of HIT-SI and HIT-SI3
8. CM Jacobson, CP12.00029 : Initial Studies of Validation of MHD Models for MST Reversed Field Pinch Plasmas
9. KJ McCollam, CP12.00030 : Comparing MHD simulations of RFP plasmas to RELAX experiments
10. JP Sauppe, CP12.00031 : Analysis of Helicities and Hall and MHD Dynamo Effects in Two-Fluid Reversed-Field Pinch Simulations
11. T Bechtel, CP12.00068 : High-beta extended MHD simulations of stellarators with Spitzer resistivity
12. DA Maurer, CP12.00068 : High-beta extended MHD simulations of stellarators with Spitzer resistivity
13. J Hebert, CP12.00072 : NIMROD Modeling of CTH Current Rise Dynamics
14. N Roberds, CP12.00075 : Simulations of Sawtooth Oscillations In CTH
15. VV Mirnov, CP12.00090 : Analytical and numerical treatment of drift-tearing and resistive drift instabilities in plasma slab
16. EB Hooper, GP12.00073 : Nonaxisymmetric effects in strongly driven Coaxial Helicity Injection in simulations of NSTX
17. ET Hinson, GP12.00117 : Physics of Plasma Cathode Current Injection During LHI
18. KJ Bunkers, NP12.00014 : Numerical Simulations of Hot Vertical Displacement Events
19. T Cote, NP12.00015 : The effect of strong radial variation of the diamagnetic frequency on two-fluid stabilization of edge localized MHD instabilities
20. EC Howell, NP12.00016 : Two-Fluid Calculations of the 1/1 Internal Kink
21. AL Becerra, NP12.00019 : NIMROD studies of RWM stability and non-linear evolution for NSTX equilibria
22. P Zhu, NP12.00024 : Plasma Response to Resonant Magnetic Perturbation in a Tokamak
23. X-T Yan, NP12.00025 : Neoclassical Toroidal Viscosity Induced by Resonant Magnetic Perturbation in Tokamak Edge Plasma
24. Z-Q Hu, NP12.00026 : Kinetic MHD Simulations of Shear Alfv\'{e}n Waves Driven by Fast Particles in a Tokamak
25. M Halfmoon, NP12.00036 : Energetic Ion Interactions with Tearing Mode Stability
26. S Kruger, NP12.00039 : NIMROD Modeling of Sawtooth Modes Using Hot-Particle Closures
27. F Ebrahimi, PO6.00002 : Full flux closure and equilibrium state during simulations of Coaxial Helicity Injection in NSTX-U
28. S-C Yang, PP12.00071 : Two-fluid MHD Regime of Drift Wave Instability
29. JR King, TP12.00104 : Accurate Experiment to Computation Coupling for Understanding QH-mode physics using NIMROD

A new approach makes better use of the linear relation between Ψ and j_ϕ.

- As with outer-loop updates, we use Biot-Savart to provide a linear relation between current and magnetic flux.

$$\Psi(R,Z) = -\frac{\mu_0 R}{2} \iint \underbrace{\oint \underbrace{\frac{\cos\phi' d\phi'}{|\mathbf{x}-\mathbf{x}'|}}_{\text{Evaluate analytically like a coil.}} j_\phi(\mathbf{x}') dR' dZ'}_{\text{Evaluate through Gaussian integration.}}$$

Evaluate analytically like a coil.

Evaluate through Gaussian integration.

- The flux is needed at boundary nodes and is found from current-density values at quadrature points. [J_q is the Jacobian at point q.]

$$\Psi_{node} = -\frac{R_{node}}{2} \sum_q \left(\oint \frac{\cos\phi d\phi}{|\mathbf{x}_{node} - \mathbf{x}_q|} \right) (\mu_0 R j_\phi)_q w_q J_q$$

or $$\underline{\Psi} = \underline{\underline{M}}\, \underline{j}$$

vector of current density values at quadrature points

vector of flux values at boundary nodes

non-square dense matrix computed at startup